RSC Advances

ROYAL SOCIETY OF CHEMISTRY

www.rsc.org/advances

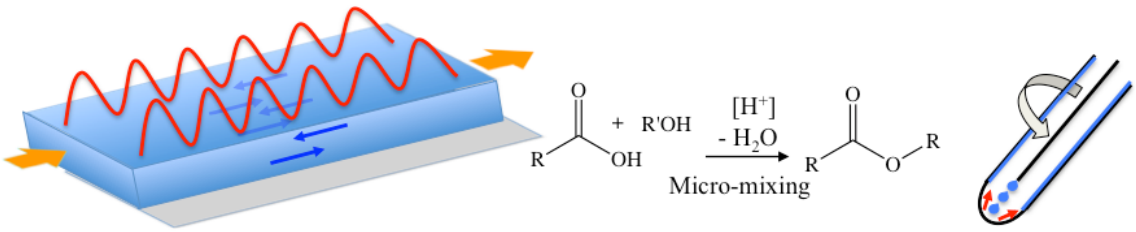

Organic synthesis under shear : High yielding, acid catalysed, continuous flow synthesis of esters involves coupling of vibrations in thin film fluidics, as rapid environmentally friendly organic methodology.

RSCAdvances RSCPublishing

ARTICLE

Continuous flow Fischer esterifications harnessing vibrational-coupled thin film fluidics†

Cite this: DOI: 10.1039/xoxxoooooox

J. Britton [a], S. B. Dalziel [b] and C. L. Raston [a*]

Received ooth January 2012,
Accepted ooth January 2012

DOI: 10.1039/xoxxoooooox

www.rsc.org/

Rapid Fischer esterification reactions occur under solventless, continuous flow conditions in dynamic thin films. They use limited catalyst, require no additional heat input and occur within the confinements of an inexpensive vortex fluidic device (VFD). The associated mechanoenergy is primarily delivered from two types of vibration, which are manifested in sharp increases in yield of the reactions. These vibrations promote the existence of Faraday waves that alter the instantaneous shear rates of the reactants within the rotating tube. Tuning the rotational speed of the device allows harmonic vibrations to be utalised in the synthesis of alkyl-based esters within both a high and low contact angle NMR tube.

Introduction

Reactions of alcohols with carboxylic acids to form esters are fundamentally important in organic synthesis. Typically, these esterification reactions require an acid catalyst to promote the electrophilicity of the carbonyl moiety,[1a] with heating improving the kinetics.[1b] As chemistry has progressed, so has the diversity and complexity of such catalysts, with the ability to generate esters in excellent yields.[2-6] Nevertheless, the inherent complexity, associated expense of such processing and the safety of large scale batch processing can be questionable, as can the difficulties in scaling up. To this end we have developed high yielding esterification reactions, where the chemistry is simplified, using continuous flow processing and simple acid catalysts within the confinements of the recently developed vortex fluidic device (VFD).[7] This thin film microfluidic platform allows the continuous flow processing of fluids up to 7 mL/min or 20 mL/min for the 7.0 mm or 17.5 mm internal diameter borosilicate tubes (commercially available sizes of NMR tubes) respectively, Figure 1. Scaling up is possible by using parallel arrays of such inexpensive VFD, as in conventional microfluidic processing involving channels. In this context, clogging is not an issue for the VFD, as it can be for other microfluidic processing platforms.[8]

Esterification reactions are widely used in industry, including the synthesis of alkyl-acetate based esters and fatty acid esters as in biodiesel production. Butyl acetate alone is an important component in coatings, having a relatively low vapour pressure, featuring as a solvent for polymerization reactions and as a fragrance in cosmetics.[9,10] Currently, advancing the production of esters (especially for biodiesel) focuses around microbial lipases and oleaginous microorganisms,[11-12] with other processes using ion exchange resins [13] and heterogeneous catalysts such as MgO [14] and Na_2CO_3.[15] While these systems are highly effective, there is a number of concerns, including the generation of a waste stream, catalyst lifetime, the use of high temperatures and pressures, and rather specific conditions required for biological catalysts. In addition, Lewis acid catalysts, for example, tin-octoate, require removal after processing.[9] Overall, developing more versatile and more benign alternative reactions, using smaller amounts of catalyst at standard temperature and pressure, with lower environmental impact and capital outlay are warranted.[16, 17]

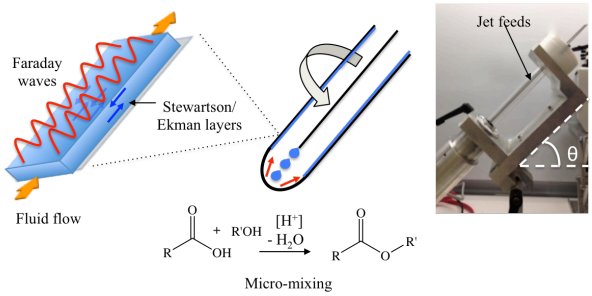

Figure 1. Photograph of a vortex fluidic device (VFD) housing a 17.5 mm internal diameter borosilicate glass NMR tube at a 45 degree angle, θ, relative to the horizontal position, along with a schematic of the dropping regime in the VFD and the subsequent dynamic thin film. The liquid is introduced into the system through the metal jet feeds, the liquid

then whirls up the rotating tube and exits through a teflon channel in the housing unit at the top of the device. Full schematics and workings of the device have been reported previously.[7]

The VFD can operate under so call continuous flow mode where jet feeds deliver liquid to the base of the rapidly rotating tube leading to intense shearing and micromixing in the resulting dynamic thin film, with the film thickness primarily governed by the rotational speed, flow rate and tilt angle, θ, of the tube. Controlling the delivery of a drop of liquid onto the hemispherical bottom of the VFD tube sets the level of shearing and when the liquid exits the hemisphere, a helical wave is formed, which is likely to provide additional shearing due to the viscous drag of the liquid against the rotating tube. The intense shear that is created at the base of the tube is also present in the thin film, which arises from the Stewartson/Ekman layers.[18] Also noteworthy, is that the intense shear can result in a change of the surface tension of the thin film, which can facilitate high mass transfer of gases into and out of the liquid.[19]

The VFD is a versatile processing platform in materials chemistry, for example, in exfoliating graphene and *h*-BN, [20] coating algal cells with graphene and a magnetic polymer,[21] controlling the pore size of mesoporous silica [22] and decorating graphene with palladium nano-particles.[23] In the context of the present study, the VFD is effective in enhancing the dimerization of cyclopentadienes, the direct base catalysed synthesis of 2,4,6-triarylpyridines from aromatic aldehydes and ketones in a single pass,[7] the stereospecific synthesis of calixarenes derived from resorcinol or pyrogallol and aldehydes,[24] and room temperature conversion of sunflower oil to biodiesel,[25] all under continuous flow conditions. The work herein focuses on furthering the fundamental organic chemistry, with an aim of understanding the remarkable outcome of the above reactions carried out using the device.

Results and discussion

The temperature change (ΔT) of the thin film in the VFD operating in confined mode operation was monitored for 2 mL of *n*-butyl acetate, to ascertain any temperature change associated with varying the θ and rotational speed, Figure 2. The choice of θ dramatically affects the temperature of the thin film, with a distinct change from 5000 rpm to 5250 rpm at θ of 45°, for the device operating at ambient temperature (17.5 mm internal diameter tube). After three minutes at these operating parameters ΔT was + 7.73 °C (IR thermal imaging), which is 3.33 °C greater than ΔT at 5000 rpm. This value is large in comparison to ΔT ~ +1 °C at a θ 30 ° or 60 ° when stepping from 5000 to 5250 rpm, Figure 2. In contrast, at θ 30° the highest +ΔT corresponds to the step from 5500 to 6000 rpm, regaining the linear increase in temperature. For all angles and speeds > 6000 rpm, the higher the rotational speed, the greater +ΔT. The vibration of the glass tube within the upper housing unit whilst rotating leads to the generation of frictional heat, Figure 2, which is transferred into the thin film through the rotating glass tube. At certain rotational speeds there are more or larger vibrations that lead to increased amounts of friction, thus leading to greater heat transfer into the thin film, especially at 5250 rpm where there is a sharp +ΔT. The sharpness of this increase in temperature is due to a more effective vibration of the rotating tube against the teflon housing unit. At certain rotational speeds, the vibration of the glass tube will fall into what one may call a harmonic, and this will generate more heat *via* friction. Thus, at 5250 rpm, for a 17.5 mm internal diameter tube, the rotational speed generates a harmonic vibration, dramatically affecting the increase in frictional heat generated (as well as chemical reactivity, see further on). As a control, the heat transfer was monitored for a rotating tube devoid of any solvent (ESI), and while heat was produced at both the upper and lower parts of the device, like in Figure 2, it remains essentially localised around the teflon housing for prolonged periods. Thus, the vibration of the glass tube against the teflon housing results in some localised heating. However, when solvent is present in the tube at the harmonic vibration, heat is dispersed throughout the glass tube, as shown in Figure 2C. This further highlights a strong fluid dynamical response at selected rotational speeds, and such vibrational effects are clearly observed at a 5250 rpm rotational speed at θ 45, Figure 2.

The continuous flow mode of the VFD was initially explored for the synthesis of *n*-butyl acetate. For comparison, as a control experiment, the batch processing reaction catalysed by sulphuric acid at room temperature was carried out, reaching ≤ 47 % conversion after 3 hours of vigorous stirring at 1400 rpm. To achieve higher conversion rates of *n*-butyl acetate, literature reports require heating between 90 - 110 °C for a number of hours.[26-29] These elevated temperature methods include the use of complex and expensive catalysts such as sulfonic acid functionalised MIL-101,[26] silicotungstic acid on bentonite,[27] expansible graphite,[28] tin oxide[29] and calcium chloride coupled with energy intensive microwave radiation.[30] Nevertheless, batch processing is still limited to diffusion control and the need to address environmental impacts remains. Herein we present an ambient pressure and temperature, continuous flow process for the synthesis of *n*-butyl acetate, which harnesses mechanoenergy in the VFD, increasing the yield (and also for other alkyl esters) by 26 % in 3.25 minutes, which is the residence time of the reactants in the tube.

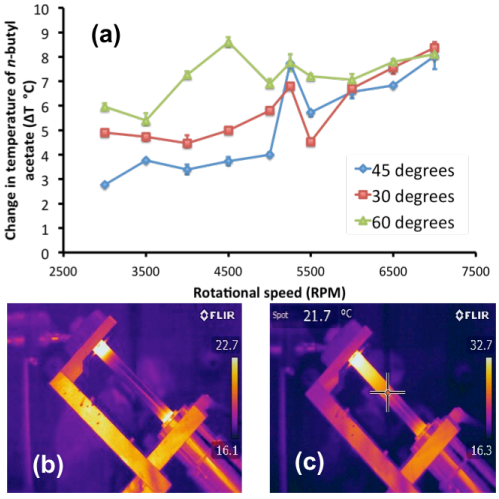

Figure 2. (a) Variation in the temperature (ΔT) of *n*-butyl acetate processed in the VFD operating in the confined mode (2 mL of *n*-butyl acetate, 17.5 mm internal diameter tube), for different rotational speeds, at θ 30 °, 45 ° and 60 ° (data points in triplicate), with the temperature measured using a thermal imaging camera (0.20 K resolution) before and after three minutes of rotation. Temperature change of n-butyl acetate was measured before and then immediately after processing, rather than measuring the temperature of the tube during processing, acknowledging that the tube is not IR transparent. (b) and (c) Thermal images after three minutes processing for 4000 and 5250 rpm respectively, at θ 45 °,

measuring the temperature of the NMR tube itself. See experimental for further details.

Both the concentration of acid catalyst and the flow rate were systematically varied for θ 30 °, 45 ° and 60 °, at

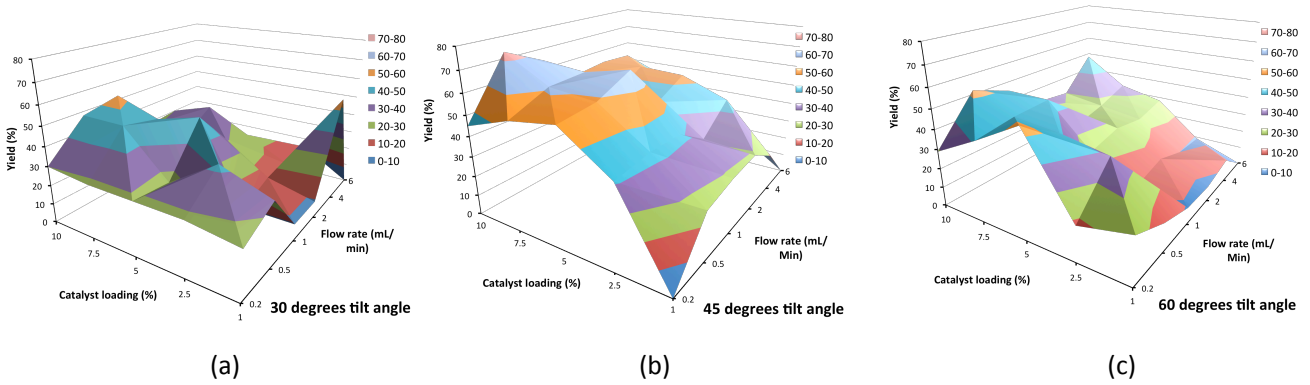

Figure 3. Percent formation of *n*-butyl acetate in the VFD (17.5 mm internal diameter NMR tube) at room temperature, as a function of flow rate and percent catalyst for θ (a) 30 °, (b) 45 ° and (c) 60 ° relative to the horizontal position, at 5250 rpm (data points in triplicate). The tilt angle θ, Figure 1, was measured by a digital protractor with a resolution of 0.01 °.

rotational speed of 5250 rpm, corresponding to the largest +ΔT, Figure 3. The increase in conversion at θ 45 ° to 73 % was the most striking for a single pass at 0.50 mL/min using 10 % acid catalyst. Conversions approaching this level were also observed for higher flow rates and lower catalyst loading. Logically, the vibrations causing the change in temperature of the system are also responsible for the overall increase in yield at a 45 ° tilt angle. This is further manifested when taking into consideration the relatively small ΔT at 30 and 60 ° tilt angles, and the overall lower yield of *n*-butyl acetate at these angles for a rotational speed of 5250 rpm, where there are no apparent vibrations. Even though this system requires no additional input of temperature, the increase in temperature of the glass, due to vibrational induced friction, has little impact on the increase in yield. This is observed when analysing the longer residence times (slower flow rate), which almost always leads to a decrease in yield. Clearly the small rise in temperature of the system is not a substantial driving force behind the reaction. This is further demonstrated for higher rotational speeds, Figure 4. The largest +ΔT is at 7000 rpm, Figure 2, but this is not a vibrational effect. Heat is generated by the fast rotating bearings, but the lack of a distinct heat change corresponds to some of the lowest yields.

Given that a tilt angle of 45 ° and a 0.50 mL/min flow rate gave the highest yield, the reaction was further optimized with these parameters fixed. A 1:1.5 ratio of *n*-butanol: acetic acid was used so that excess acid could be easily removed, and this was subsequently shown to give the highest yield (ESI), and thus the use of the VFD does not follow a simple linear relationship between ratio of reactants (as a measure of relative concentrations) and overall conversion. Other acid catalysts were tested (ESI), establishing sulphuric acid being the most efficient, with concentrated nitric, hydrochloric and phosphoric acid dramatically reducing the yield.

The collected reaction mixture was recycled through the VFD up to four times in an attempt to increase the conversion, noting that starting material was still present in the product mixture after a single pass through the VFD (ESI). Interestingly, this recycling resulted in some evaporation and a decrease in the amount of product isolated. Clearly, an important processing parameter for the VFD is residence time, which is controlled by the flow rate, which was set at 0.50 mL/min after establishing that it results in the highest ester formation at the tilt angles explored.

Finer control of the reaction was studied by varying the rotational speed, noting that as the rotational speed increases, the thickness of the dynamic thin film in the VFD decreases, as established for the confined mode of operation,[7] and presumably this also prevails under the continuous flow mode. For ≥ 4500 rpm there is a general decrease in yield, arising from a small amount of evaporation of the reactant components, as the film gets thinner, Figure 4. However, at 5250 and 6000 rpm the yield is dramatically higher, for a very narrow speed range (+/- 10 rpm) for a 17.5 mm internal diameter tube supported by a single bearing system, with the top of the tube contained within a 20.51 mm guide, having a headroom of 0.51 mm. The sharpness of the peaks at 5250 and 6000 rpm indicate that a mechanical resonance is responsible for the increase in yield, driving a Faraday wave like fluid dynamic response.[31] The VFD dramatically amplifies the synthesis of the ester when a mechanical response is present. This Faraday wave enhancement occurs at the rotational speeds indicated above; for all other rotational speeds tested, there seems to be no additional mechanical enhancement.

In further testing the presence of macro-vibrations between the glass tube and the housing chamber, a double bearing VFD system was constructed with the top of the tube now also supported by a bearing. This resulted in the peak at 5250 rpm disappearing, but the peak at 6000 rpm remaining, with the overall yield decreasing slightly. Thus, the 5250-rpm peak arises from macro-vibrations imparting additional mechanical energy to the NMR tube. However, new peaks emerge 250 rpm apart, at 6250 and 6500 rpm, when using the double bearing system, indicating that this is an ordered form of mechanical energy, and is consistent with a harmonic micro-vibrational effect. The 7.0 mm internal diameter (external diameter, 10.0 mm) VFD processor was also used for comparison, at the same flow rate, which reveals a similar pattern, but with different rotational speeds producing sharp increases in yields, centred around 4510 and 6490 rpm. The VFD unit housing the smaller

diameter tube also gives the rotating tube a small head room within the housing unit at the top of the device, and the peak at 4510 rpm is indicative of a strong macro-vibration of the borosilicate tube against the housing chamber. This vibrational model is also consistent with the thermal IR images, Figure 2, which show a large amount of heat being generated at the upper bearing, arising from macro vibrational induced friction of the NMR tube against the teflon sleeve. The 7.0 mm tube also has a peak at 6490 rpm, close to the 6500 rpm for the 17.5 mm tube.

When the vibration at 5250 rpm was removed for the 17.5 mm tube, the chemical enhancement was also removed. This presumably arises from a change in the stability of the thin film, thereby revealing new peaks at 6250 and 6500 rpm. However, at 6010 rpm with a flow rate of 0.50 mL/min there is a large decrease in yield, and thus the vibration here appears to have a detrimental effect on the stability of the thin film as further described below, or that the window for the vibration is small. There were no sharp increases in yield, but nevertheless there is a vibrational effect on the thin film at 6010 rpm, as for all other studies using the 17.5 mm internal diameter NMR tube.

The fluid based mechanism on how vibrations cause large increases in yields relates to the stability of the thin film. Vibrations within the tube are likely to excite Faraday waves through a modulation of the large centrifugal force experienced by the film on the walls of the rapidly rotating tube, altering the instantaneous shear rates. Strengthening this theory further is that for both the continuous flow synthesis and confined mode heating of *n*-butyl acetate, Figures 2 and 4 respectively, for a single bearing system, the optimum rotational rate was 5250 rpm. The similarity of optimum rotational speed provides further evidence that this is a mechanical resonance of the system. Further to this model, if there is too much vibration then the thin film breaks up changing the dynamics, resulting in reduced shear stress, leading to a decrease in yield. This was observed for an inadvertently corroded bearing, with high levels of noise and vibration resulting in a 35 % decrease in yield.

The conversion to *n*-butyl acetate was typically lower in the 7.0 mm VFD for the same flow rate, and this relates to the lower surface area and thus the decrease in residency time of the thin film relative to a 17.5 mm tube. There is an expected optimum radius associated with the VFD tubes, noting that the radius at which the drop hits the bottom of the tube sets the maximum amount of shear possible. However, the dominant effect is the residency time of the fluid in the hemisphere at the bottom of the tube. There is conceivably an optimum between the impact drop radii and residency time within the hemispherical part of the VFD tube. We also note that changing the flow rate did not disrupt the position of these peaks, further indicating a mechanical resonance driving a secondary fluid dynamical response that can exist due to the rapid rotation of the VFD tube.

The optimised parameters for preparing *n*-butyl acetate were used for preparing a range of esters, without further individual optimisation, so that a direct comparison could be drawn, Table 1. However, an additional operating parameter was introduced, namely varying the nature of the inner surface on the NMR tubes, with the internal surface of the 17.5 mm VFD tube being coated with dodecyl alkyl silane, thereby creating a hydrophobic surface, as opposed to a hydrophilic surface for the as received NMR tubes (ESI). While some yields decreased for the hydrophobic surface, the yield of *n*-butyl acetate increased to 80 % and the yield of *n*-hexyl propionate and *n*-hexyl acetate increased by 33 % and 9 % respectively. The decrease in yields of the other esters presumably arises from the established film at the bottom of the tube becoming unstable for a hydrophobic surface, leading to a decrease in sustained shear, and thus a decrease in reactivity. Surprisingly *n*-hexyl alcohol rather than the loner chain *n*-octyl alcohol benefits the most from the hydrophobic coating, The ability to change a number of processing parameters suggests that esterification reactions can be further improved on an individual basis.

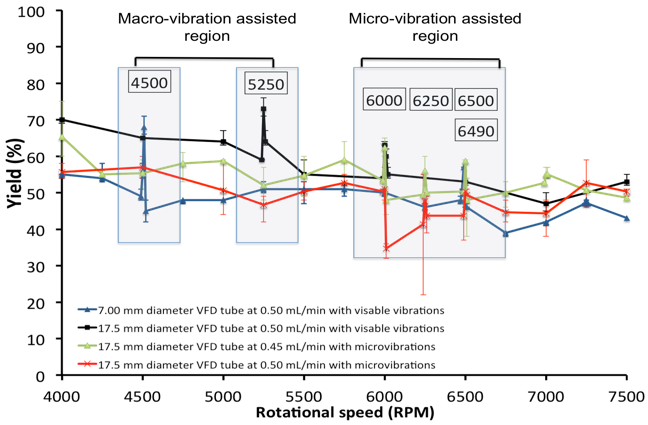

Figure 4. Variation in yield of n-butyl acetate in 7.0 mm and 17.5 mm internal diameter tubes in the VFD with either single or double bearings. Single bearing regions are highlighted as macro-vibrational effects and double bearing effects are highlighted as micro-vibrational regions, with θ 45° for varying flow rates (data points in triplicate).

Conclusions

We have identified vibrations in two different diameter VFD units which transfer additional mechanoenergy into the thin film, which is manifested in an increase in yield by ≤ 26 %, to >70% for *n*-butyl acetate, for a single pass for which the residence time is 3.25 minutes. This is in contrast to 47 % yield of *n*-butyl acetate for a three hour room temperature batch reaction. The increase in yield is without the need for any further modification to the VFD or the surface of the glass tubes. It must be noted that these vibrations are not confined to a single system, with several systems all giving reproducible results at the rotational speeds indicated. Even though the measurements of yield were carried out offline, the reaction was quenched on exit of the system, thus providing an accurate measurement of conversion. Overall, the results highlight the versatility of the inexpensive VFD beyond earlier studies, now with a clearer understanding of the repertoire of operating parameters, which can be translated to reducing the environmental impact of synthesis due to the minimisation of energy requirements and the just in time process of operation.

Table 1. Yields of esters prepared using the VFD operating at θ 45^0, 5250 rpm, for a 17.5 mm internal diameter tube (borosilicate glass or its dodecyl silane treated analogue), with an alcohol: acid ratio of 1: 1.5, for a flow rate of 0.50 mL/min, which corresponds to 3.25 min residence time.

Ester	Yield (%) for borosilicate glass surfaces	Yield (%) for silane treated surfaces
n-propyl acetate	40	29
n-butyl acetate	73	80
n-pentyl acetate	87	59
n-hexyl acetate	89	98
n-octyl acetate	82	70
n-butyl propionate	77	73
n-pentyl propionate	55	62
n-hexyl propionate	57	90
n-propyl propionate	79	49
i-propyl propionate	33	2
s-butyl acetate	36	6
s-butyl propionate	28	11

Experimental

The required carboxylic acid (1.5 eq.), alcohol (10 mL, 1.0 eq.) and acid catalyst (0.1 eq.) were stirred for 2 minutes. The solution was then added to the VFD using a computer controlled syringe pump at a flow rate of 0.50 mL/min with the 17.5 mm internal diameter (20.0 mm outside diameter) or 7.0 mm internal diameter tube (10.0 mm external diameter) rotating at a specified speed and tilt angle, θ. The solution was collected and added to saturated sodium bicarbonate (2 M, 10 mL) in quenching the reaction, and the resultant solution was washed further with cold water (2 x 10 mL), dried using $MgSO_4$ and filtered to afford colourless liquids. Yields were calculated and any remaining alcohol in the sample was detected using ^{1}H NMR spectroscopy. Yields were adjusted in accordance with the ratio between the CH_2 triplet peak of *n*-butanol acetate at 4.01 ppm and the CH_2 triplet peak of the *n*-butyl alcohol component of the ester at 3.59 ppm. Initial ^{1}H NMR spectra were recorded using typical quantitative NMR conditions (Delayed pulsing (D1) = 10.00, number of scans (ns) = 64), however subsequent spectra were obtained normally (D1 = 1.00, ns = 16) with no observable differences. All esters had identical spectra to those previously reported. See supplementary information for the method for hydrophobic coating of the tube (ESI).

Temperature measurements were carried out with a high level of confidence using a FLIR-T62101 thermal imaging camera with a resolution of 0.02 K. The camera was calibrated using radiation sources that are traceable to National Standards at the SP Technical Research Institute of Sweden, or to NIST, National Institute of Standards and Technology (USA). Measurements were in triplicate, with the largest error 0.37 °C, and were determined from the difference in temperature of the fluid tens of seconds before the experiment (outside of the tube) and immediately after processing, thus allowing an accurate measurement of the temperature of the thin film.

Notes and references

[a] School of Chemical and Physical Sciences, Flinders University, Bedford Park, Australia, SA 5042
[b] Department of Applied Mathematics and Theoretical Physics, University of Cambridge, UK, CB3 0WB.
† This research was supported by Flinders University, the University of Cambridge, the Government of South Australia and the Australian Research Council.
Electronic Supplementary Information (ESI) available: See DOI: 10.1039/b000000x/

1 (a) J. Clayden, N. Greeves, S. Warren and P. Wothers, in *Organic Chemistry*, Oxford University Press, Oxford, 2001, pp. 280. (b) J. Clayden, N. Greeves, S. Warren and P. Wothers, in *Organic Chemistry*, Oxford University Press, Oxford, 2001, pp. 305.
2 Y. C. Sharma, B. Singh and J. Korstad, *J. Biofuel. Bioprod. Bior.,* 2011, **5,** 69-92.
3 A. L. Cardoso, S. A. Fernandes, R. Natalino, M. J. da. Silva and E. V. V. Varejão, *Catal. Sci. Technol*, 2014**, 4,** 1369-1375.
4 K. Tanabe and W. F. Hölderich, *Appl. Catal: A General*, 1999**, 181,** 399-434.
5 J. Otera, N. Danoh and H. Nozaki, *J. Org. Chem*., 1991, **56,** 5307-5311.
6 B. L. A. Prabhavathi Devi, N. Lingaiah, R. B. N. Prasad,, P. S. Sai Prasad, S. Ramu, and I. Suryanarayana, *Appl. Catal: A General*, 2004, **276,** 163-168.
7 L. Yasmin, X. Chen, K. A. Stubbs and C. L. Raston, *Sci. Rep.*, 2013, **3,** 2282.
8 X. Chen, N. M. Smith, K. S. Lyer and C. L. Raston, *Chem. Soc. Rev*, 2014**, 43,** 1387-1399.
9 J. Gangadwala, A. Kienle, S. Mahajani, S. Mankar and E. Stein, *Ind. Eng. Chem. Res.,* 2003, **42,** 2146-2155.
10 M. F. Doherty, M. F. Malone and G. Venimadhavan, *Ind. Eng. Chem. Res*, 1999, **38,** 714-722.
11 S. Benjamin, N. A. Pandey, N. Kreiger, C. R. Soccol, V. T. Soccol and P. Nigam, *Biotechnol. Appl. Biochem*, 1999, **29,** 119-131.
12 N. Qingjuan, X. Meng, J. Yang, M. Xian, L. Zhang, Q. Nie and X. Xu*, Renew. Energ*., 2009**, 34,** 1-5.
13 M. B. Bochner, S. M. Gerber, A. J. Rodger and W. R. Vieth, *Ind. Eng. Chem. Fundamen*., 1965**, 4,** 314-317.
14 L. Pengmei, E. Santacesaria, M. D. Serio and R. Tesser, *Energy Fuels*, 2008, **22,** 207-217.
15 Y. C. Sharma, B. Singh and J. Korstad, *Fuel,* 2011, **90,** 1309-1324.
16 J. A. Glaser, *Clean Technol. Envir*., 2009, **11,** 371-374.
17 R. A. Sheldon, *Chem. Soc. Rev*., 2012, **41,** 1437-1451.
18 H. P. Greenspan, *The Theory of Rotating Fluids,* Cambridge University, Press, Cambridge, 1968, p 327.
19 X. Chen, F. Yasin, P. Eggers, R. Boulos, X. Duan, R. Lamb and C. L. Raston, *RSC Adv.,* 2013. **3,** 3213-3217.
20 M. H. Wahid, E. Eroglu, X. Chen, S. Smith and C. L. Raston, *Green Chem.*, 2013, ***15,*** 650-655.
21 M. H. Wahid, E. Eroglu, X. Chen, S. Smith and C. L. Raston*, RSC Adv*., 2013, **3,** 8180-8183.
22 C. L. Tong, R. Boulos, C. Yu, K. Lyer and C. L. Raston, *RSC Adv*., 2013, **3,** 18767-18770.
23 X. Chen, W. Zang, K. Vimalanathan, K. Lyer, and C. L. Raston, *Chem. Commun*., 2013, **49,** 1160-1162.
24 L. Yasmin, T. Coyle, K. A. Stubbs and C. L. Raston, *Chem Commn.,* 2013, **49,** 10932-10934.
25 J. Britton and C. L. Raston, *RSC Advances*, 2014, DOI: 10.1039/C4RA10317C
26 Y. Zang, J. Shi, F. Zhang, Y. Zhong and W. Zhu, *Catal. Sci. Technol.,* 2013, **3,** 2044-2049.
27 J. Z. Jin, *Advanced Materials Research,* 2012, **362,** *550-553*.
28 X. Y. Pang, *Journal Of Chemistry,* 2014**, 4,** 1816-1822.
29 H. Guo, *Huaxue Yanjiu Yu Yingyong,* 2010**, 6***, p* 678.
30 Y-X. Liu, Huaxue Gongye Yu Gongcheng, 2010**, 1,** p 17.
31 K. Kumar*, Proc. R. Soc. Lond. A*., 1996, **452,** 1948.